Materials Horizons

ROYAL SOCIETY OF CHEMISTRY

COMMUNICATION

View Article Online
View Journal

Cite this: DOI: 10.1039/d5mh01986a

Received 20th October 2025,
Accepted 4th February 2026

DOI: 10.1039/d5mh01986a

rsc.li/materials-horizons

Targeted metabolic glycoengineering using multivalent mannosyl metal–organic frameworks (MOFs)

Pei-Hong Tong, †[a] Chen Guo,†[ac] Xi-Le Hu,[a] Tony D. James, *[de] Jia Li *[c] and Xiao-Peng He *[ab]

Cell-type selective metabolic labeling of glycans in complicated biological environments remains a big challenge. Herein, we develop a glycan labeling tool by encapsulating a non-natural azido sugar (ManNAz) into a mannosyl ligand-modified metal–organic framework (MOF) (MIL-101-Man). The mannosyl ligands multivalently displayed on the surface of the MOFs bind specifically to mannose receptors (MRs) expressed on the surface of a target cell to mediate targeted delivery of the unnatural sugar. Upon endocytosis, exposure of the MOFs to the acidic environment of the endosomes and lysosomes resulted in the release of ManNAz to subsequently undergo metabolic incorporation into cellular glycans. A series of biological experiments followed by fluorescence-based biorthogonal cell labelling demonstrated the receptor-dependent uptake of MIL-101-Man, and an assay involving the co-culture of two cell lines in one cellular medium confirmed the target specificity of the MOFs for the glycoengineering of target cells that overly express MRs over adjacent control cells with minimal MR expression. This study offers an effective tool for the metabolic glycoengineering of cells in a receptor-targeting manner.

New concepts

This work offers an effective tool for the metabolic glycoengineering of cells in a receptor-targeting manner, aiming to address the key challenge of cell-type selective metabolic labeling of glycans in complex biological environments. A mannosyl MOF carrier was developed in which surface-anchored mannose ligands act as receptor-targeting agents for cell-surface MR multivalent interactions, enabling targeted delivery of the metabolic sugar probes. Fluorescence-based biorthogonal cell labelling confirmed the receptor-dependent uptake of the mannosyl MOFs, and the co-culture of two cell lines in one cellular medium confirmed the target specificity of the MOFs, thereby enabling the glycoengineering of target cells that overly express MRs. The ability of our multivalent glycosyl MOF system to achieve glycoengineering of a target cell in a bicellular system highlights its potential for glycobiological studies in complex biological samples. Notably, this is the first study to achieve the delivery of unnatural sugars for metabolic glycoengineering through the construction of mannosyl MOFs, which exhibit the merits of tunable porosity enabling the accommodation of other non-natural sugar derivatives. Additionally, the targeting agent can be flexibly replaced with other sugars to target various sugar-binding proteins expressed on the surface of mammalian cells, providing a programmable platform for the next generation of precise cellular metabolic glycoengineering technology.

Introduction

Bioorthogonal chemistry has made great strides in labeling and manipulating the function of biomolecules *in situ*. During the labeling process, a metabolic precursor (*e.g.* an azido compound) is incorporated into a target biomolecule through natural biosynthetic pathways, and then a complementary reporter is added to react with the precursor through biorthogonal reactions enabling biomolecular labelling in live cells and animals.[1–3] As an important application of bioorthogonal chemistry, metabolic glycan labeling using unnatural sugars as the biorthogonal precursors shows great promise for applications in cell-surface glycoengineering,[4,5] targeted cancer therapy,[6,7] immunomodulation[8] and glycoproteomics analysis.[9,10] However, non-natural sugars containing biorthogonal handles (*e.g.*, an azido group) are non-selectively internalized by cells when used in complex physiological environments. Given that sugars can be processed by literally all mammalian cells that contain endogenous glycan metabolic pathways, as a result false-positive signals

[a] Key Laboratory for Advanced Materials and Joint International Research Laboratory of Precision Chemistry and Molecular Engineering, Feringa Nobel Prize Scientist Joint Research Center, Frontiers Center for Materiobiology and Dynamic Chemistry, School of Chemistry and Molecular Engineering, East China University of Science and Technology, 130 Meilong Rd., Shanghai 200237, China. E-mail: xphe@ecust.edu.cn

[b] The International Cooperation Laboratory on Signal Transduction, National Center for Liver Cancer, Eastern Hepatobiliary Surgery Hospital, Shanghai 200438, China

[c] State Key Laboratory of Chemical Biology, Shanghai Institute of Materia Medica, Chinese Academy of Sciences, Shanghai, 201203, China. E-mail: jli@simm.ac.cn

[d] Department of Chemistry, University of Bath, Claverton Down, Bath BA2 7AY, UK. E-mail: t.d.james@bath.ac.uk

[e] School of Chemistry and Chemical Engineering, Henan Normal University, Xinxiang 453007, China

† These authors contributed equally to this work.

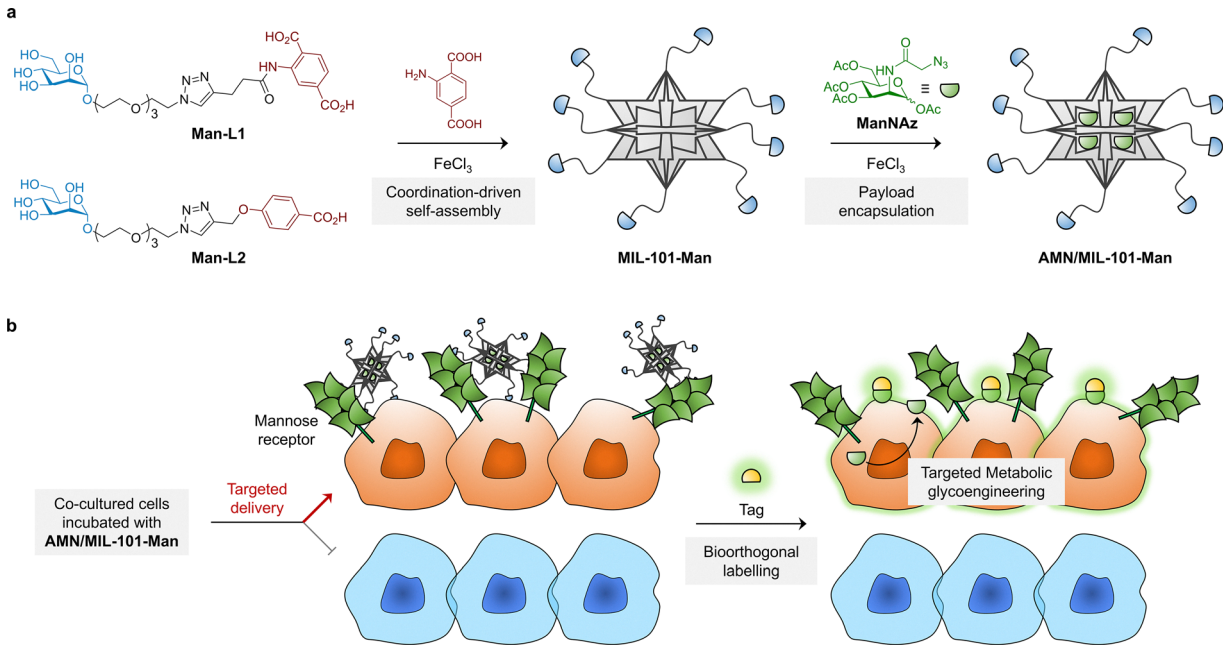

Scheme 1 Schematic illustration of the construction of mannosyl MOFs (**MIL-101-Man**) for receptor-targeted metabolic glycoengineering. (a) Structure of the mannosyl ligands **Man-L1** and **Man-L2**, and schematic illustration of the one-pot construction of **MIL-101-Man** capable of loading **ManNAz**, an unnatural sugar for metabolic glycoengineering. (b) Targeted delivery of **ManNAz** to a target cell overly expressing mannose receptors (MRs) by **MIL-101-Man** in a co-cultured system of two cell lines (one with high expression of MRs and the other with minimal MR expression) for metabolic glycan labelling using a fluorescent bioorthogonal tag.

could be produced, thus compromising labelling and therapeutic precision. Therefore, the development of carriers capable of specifically delivering unnatural sugars to a target cell has become a vital research direction in this area.[11]

For example, Chen and co-workers developed folate-modified liposomes to deliver unnatural sugars to target cells in a folate receptor-dependent manner.[12] Subsequently, the same group used ligand-modified liposomes as a carrier to deliver sugars to specific tissues, successfully achieving *in vivo* labeling and imaging of brain sialylation.[13] Additionally, Qu and co-workers constructed pH-responsive liposomes camouflaged with natural cancer cell membranes for delivering azidosugars.[14] The modified liposome targets membrane-derived cells through the homotypic recognition mechanism of surface receptors, facilitating cell entry *via* cholesterol-dependent endocytic pathways for selective glycan engineering of tumor cells. Beyond liposomal delivery systems, a recently developed biodegradable hollow manganese dioxide nanoplatform similarly achieved controlled release of unnatural sugars in the tumor microenvironment, thereby enabling tumor-specific glycan labelling.[15] Despite such progress, targeting agents used for delivery as well as material platforms in which unnatural sugars are appropriately accommodated are scarce.

As an emerging class of powerful delivery materials, metal–organic frameworks (MOFs) formed by coordination between metal ions/clusters and organic ligands have a porous structure capable of efficiently loading small molecules, and the payload release can be controlled through finely tuning the structure of the MOFs.[16–18] In addition, the surface of MOFs can be readily functionalized with targeting agents such as antibodies, aptamers and glycans, for delivery of payloads to target cells and tissues.[19–22] Glycans are widely used as targeting agents in biomedical research due to their ability to selectively bind to glycan receptors expressed on the cell surface. This interaction could then induce endocytosis of the receptor-bound cargo, and after translocation to the lysosomes, the acidic pH effectively triggers structural deformation of the MOFs for payload release.[23] Recently, Yin *et al.* reported a sugar-modified MOF system for liver-targeted delivery of doxorubicin. The system was prepared *via* post-synthetic modification of glycans on the surface of MOFs, which unfortunately compromised the structural integrity and stability of the material.[24] To the best of our knowledge, MOFs capable of the targeted delivery of unnatural sugars for metabolic glycoengineering have never been reported.

Here, we exploited a one-step method to construct multivalent mannose-modified MOFs for the targeted delivery of an unnatural azido sugar (**ManNAz**) to a target cells that overly expresses mannose receptors (MRs) (Scheme 1). Two mannosyl ligands (**Man-L1** and **Man-L2**) were synthesized and used in a one-pot assembly with $FeCl_3{\cdot}6H_2O$ and 2-aminoterephthalic acid ($H_2BDC\text{-}NH_2$) forming the mannosyl ligand-functionalized MOFs (**MIL-101-Man**) with well-controlled morphology and particle sizes. Because of their suitable porous structure, **ManNAz** was loaded into the MOFs efficiently. A series of biological experiments using fluorescence-based bioorthogonal labelling confirmed the efficacy of the delivery system for MR-targeted glycoengineering in a receptor-targeting manner.

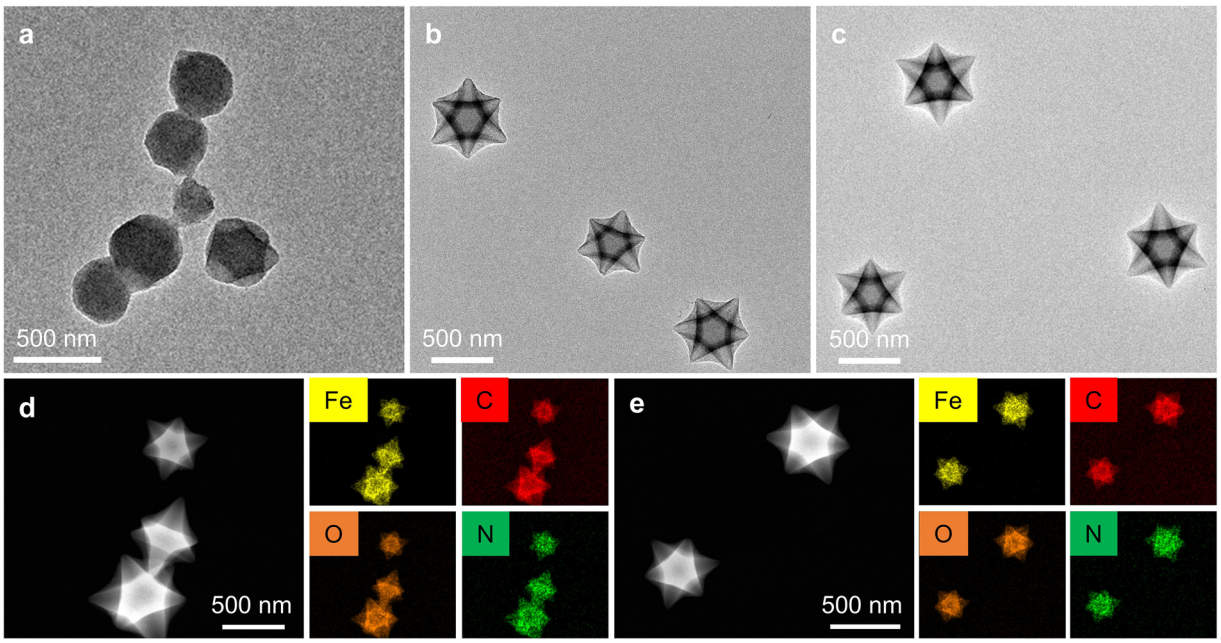

Fig. 1 Morphological characterization of **MIL-101-Man**. Transmission electron microscopy (TEM) images of (a) **MIL-101**, (b) **MIL-101-Man1** and (c) **MIL-101-Man2**. Energy dispersive X-ray (EDX) mapping analysis of (d) **MIL-101-Man1** and (e) **MIL-101-Man2**.

Results and discussion

Construction and characterization of the mannosyl MOFs

A known MOF system, MIL-101, which can be readily formed *via* coordination between $FeCl_3{\cdot}6H_2O$ and $H_2BDC\text{-}NH_2$ was used due to its biocompatibility as well as nanoscale mesoporous channels (typically 2.3–2.7 nm) suitable for accommodating small molecules.[25] To avoid the structural deformation of MOFs caused by post-synthetic modifications with targeting ligands,[26] we designed and synthesized two mannosyl organic ligands, **Man-L1** and **Man-L2** (Scheme 1a), *via* a copper(I)-catalyzed azide–alkyne click reaction between an azido mannoside and benzoic acid derivatives (Scheme S1). The mannosyl ligands **Man-L1** and **Man-L2** were directly used for a one-pot co-assembly with $FeCl_3{\cdot}6H_2O$ and $H_2BDC\text{-}NH_2$ at 60 °C for 24 h to produce **MIL-101-Man1** and **MIL-101-Man2**, respectively. **MIL-101** without the mannosyl ligands was also prepared as a control material. The as-prepared MOFs were characterized using a variety of techniques.

Transmission electron microscopy indicated that the morphology of **MIL-101** changed from irregular spheres to well-defined spiked species when either mannosyl ligand was used for assembly (**MIL-101-Man1** or **MIL-101-Man2**) (Fig. 1a–c). We thus infer that the mannosyl ligands could regulate the morphology of MOFs. Subsequently, X-ray diffraction (XRD) analysis exhibited similar crystal structures of **MIL-101-Man1** and **MIL-101-Man2** to that of **MIL-101** (Fig. S1), suggesting that the capacity of the MOFs for accommodating small molecules was not compromised by surface functionalization. Energy-dispersive X-ray (EDX) mapping (Fig. 1d and 1e) confirmed that Fe, C, O, and N elements are uniformly distributed in **MIL-101-Man1** and **MIL-101-Man2**. Scanning electron microscopic

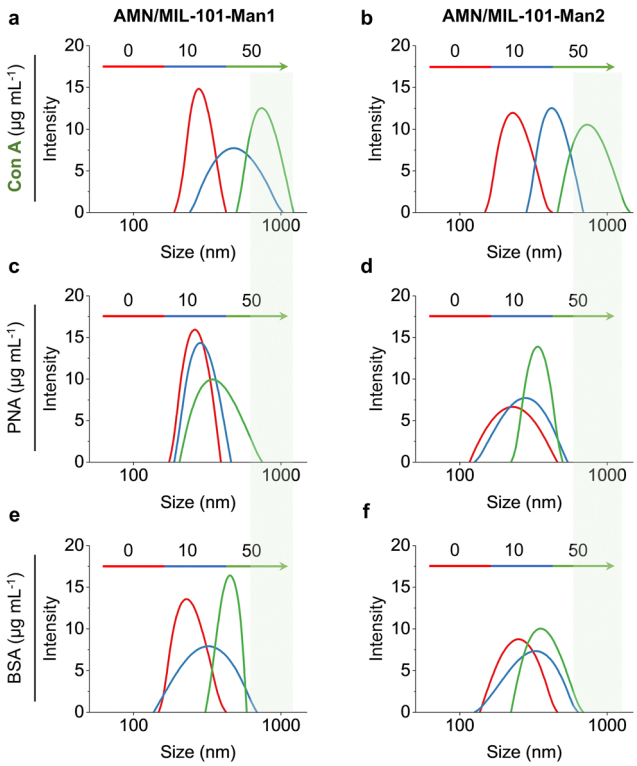

Fig. 2 Lectin-mediated agglutination assay of MOFs. Measuring the hydrodynamic diameters of **AMN/MIL-101-Man1** (50 μM/100 μg mL^{-1}) in the presence of increasing concentrations of (a) Con A, (c) PNA and (e) BSA, and **AMN/MIL-101-Man2** (55 μM/100 μg mL^{-1}) in the presence of increasing concentrations of (b) Con A, (d) PNA and (f) BSA measured by DLS in a 10 mM HEPES solution containing 0.15 M NaCl, 1 mM $CaCl_2$ and 1 mM $MnCl_2$ at pH 7.4.

(SEM) images with wide-field views illustrated the structural uniformity of **MIL-101**, **MIL-101-Man1**, and **MIL-101-Man2** (Fig. S2) and their good reproducibility from batch to batch (Fig. S3). To measure the mannose content on the surface of **MIL-101-Man1** and **MIL-101-Man2**, we used the anthrone-sulfuric acid method.[27] Establishing a standard curve (Fig. S4), the mannose content was measured to be 0.52 and 0.48 mg mL^{-1} in **MIL-101-Man1**, and **MIL-101-Man2**, respectively, indicating the successful grafting of mannosyl ligands to **MIL-101**.

We then evaluated the loading capacity of the mannosyl MOFs for **ManNAz** (*N*-azidoacetylmannosamine-tetraacylated, denoted hereafter as **AMN**) (Scheme 1a), a non-natural monosaccharide commonly used for labelling cell-surface glycans that can be metabolically converted into sialic acid derivatives.[28,29] We determined a loading efficiency of 17.8 wt% and 19.1 wt% for **MIL-101-Man1** and **MIL-101-Man2**, respectively, by high-performance liquid chromatography (HPLC) (Fig. S5). We have systematically summarized previously reported systems on metabolic sugar delivery carriers and conducted a comparative analysis between those systems and our mannosyl MOFs (Table S1). Our system possesses advantages in terms of high loading capacity, acid-responsive release, and targeted delivery of unnatural sugars, outperforming the currently reported delivery systems based on liposomes, polyethylene glycol nanoparticles, and hollow manganese dioxide carriers. The loading efficiencies determined for the mannosyl MOFs are comparable to those of previously reported **MIL-101** systems for small molecules (Table S2). While TEM indicated minimal change in their morphology after addition of **AMN** (Fig. S6), EDX analysis confirmed the existence of the payload due to an enhanced N elemental content assigned to the N atoms in **AMN** (Fig. S7). Meanwhile, the zeta potential of **MIL-101-Man1** and **MIL-101-Man2** increased after **AMN** loading, which could be ascribed to the presence of the amine group in the **AMN** structure (Fig. S8). These data confirmed the successful loading of **AMN** into the mannosyl MOFs.

Next, we evaluated the controlled release of **AMN** from mannosyl MOFs at acidic pH using dynamic light scattering (DLS) and HPLC. We found that the hydrodynamic diameter of the MOFs hardly changed when incubated in phosphate buffered saline (PBS) or Dulbecco's modified Eagle's medium-high glucose (DMEM-HG, which is commonly used for cell culture) at pH 7.4 for 24 h (Fig. S9). This suggests good stability at neutral pH. In contrast, the diameter of the MOFs gradually decreased with time when the pH of the PBS solution was decreased to 5.6 (Fig. S9). SEM images indicated that the

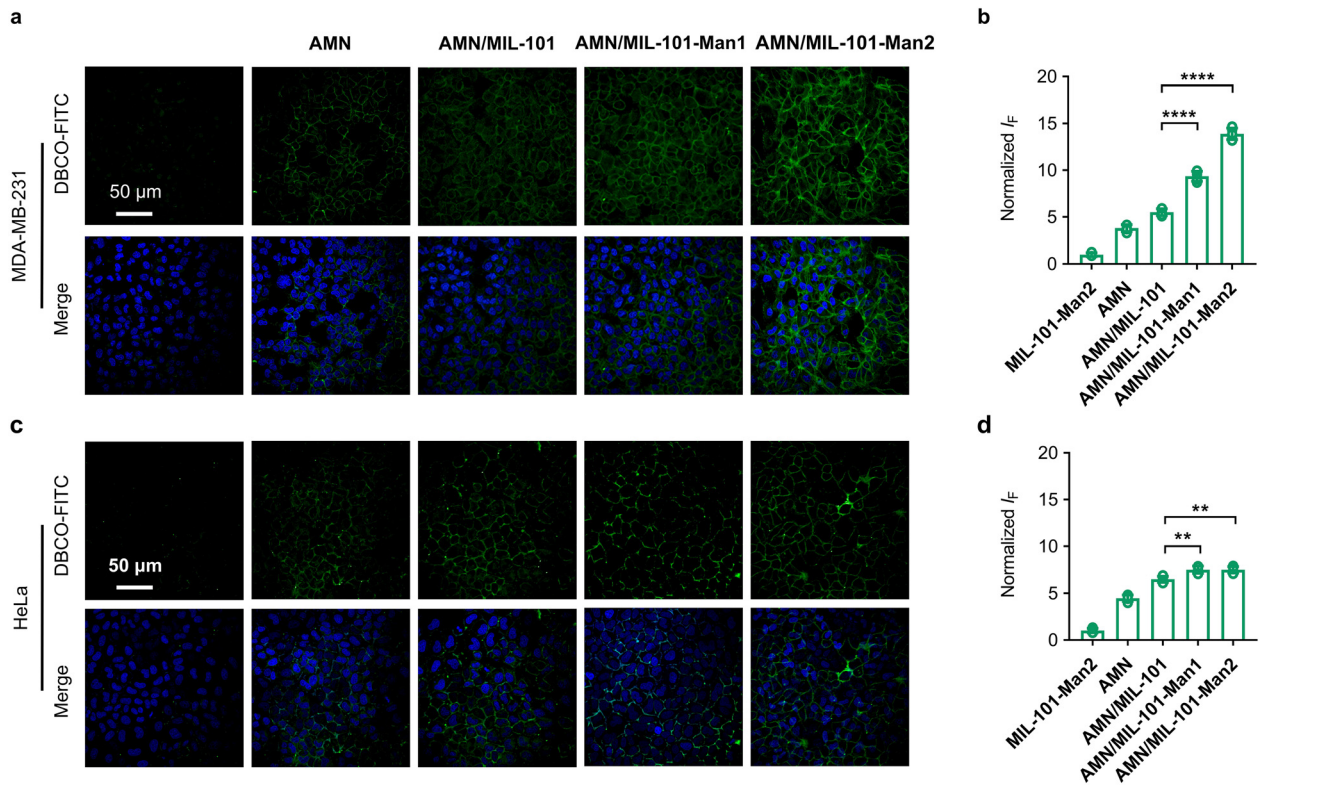

Fig. 3 Targeted metabolic glycoengineering of cells using mannosyl MOFs. (a) Fluorescence imaging and (b) quantification of MDA-MB-231 cells after treatment with **AMN** (20 μM), **AMN/MIL-101** (20 μM/35 μg mL^{-1}), **AMN/MIL-101-Man1** (20 μM/40 μg mL^{-1}), **AMN/MIL-101-Man2** (20 μM/36 μg mL^{-1}) and **MIL-101-Man2** (36 μg mL^{-1}) for 24 h with incubation, and then with **DBCO-FITC** (10 μM) for 30 min for fluorescence labelling. (c) Fluorescence imaging and (d) quantification of HeLa cells after treatment with **AMN** (20 μM), **AMN/MIL-101** (20 μM/35 μg mL^{-1}), **AMN/MIL-101-Man1** (20 μM/40 μg mL^{-1}), **AMN/MIL-101-Man2** (20 μM/36 μg mL^{-1}) and **MIL-101-Man2** (36 μg mL^{-1}) for 24 h of incubation, and then with **DBCO-FITC** (10 μM) for 30 min for fluorescence labelling. The excitation/emission channel used for **DBCO-FITC** and Hoechst 33342 is 488/500-550 nm and 405/435-480 nm, respectively. Cell nuclei were stained by Hoechst 33342. Asterisks indicate significant differences (**$P < 0.01$, ***$P < 0.001$).

original regular structures of **MIL-101-Man1** and **MIL-101-Man2** disappeared, and the particle size decreased (Fig. S10). Given that receptor-mediated endocytosis of exogeneous species is *via* endosomes (pH ~ 6.0–6.5), followed by translocation to lysosomes (pH ~ 4.5–5.5), the pH-responsive structural deformation of the MOFs ensures effective release of **AMN** intracellularly. Furthermore, HPLC was used to quantitatively analyze the pH-responsive release kinetics of **AMN** from the **MIL-101-Man2** system. As shown in Fig. S11, the released amount of **AMN** reached ~75% after 24 h at pH 5.6.

Lectin-mediated agglutination assay of MOFs

Next, we designed and carried out a lectin-based agglutination assay to evaluate the receptor-binding specificity of the mannosyl MOFs. DLS was also used to evaluate the system. Concanavalin A (Con A), which is a plant lectin known to selectively bind mannose, was used; peanut agglutinin (PNA), which binds galactose, and bovine serum albumin (BSA) were used as control. We determined a concentration-dependent hydrodynamic diameter increase for both **MIL-101-Man1** (Fig. 2a) and **MIL-101-Man2** (Fig. 2b) in the presence of increasing concentrations of Con A. In contrast, minimal changes in diameter were seen for the MOFs when PNA (Fig. 2c and d) or BSA (Fig. 2e and f) was added. These results indicate that the selective binding between Con A and the mannosyl ligands on the MOFs causes agglutination, thus providing support for their application in receptor-targeting interactions with cells.

Targeted metabolic glycoengineering of cells using mannosyl MOFs

With the mannosyl MOFs constructed, we turned our attention toward the evaluation of their cell labelling efficacy. Two cell lines, MDA-MB-231 (human triple-negative breast cancer) with a high endogenous expression level of mannose receptors (MRs or CD206)[30] and HeLa (human cervical cancer) with minimal MR expression, were selected for the labelling experiments. We first determined that the mannosyl MOFs **MIL-101-Man1** and **MIL-101-Man2** exhibited negligible cytotoxicity for both MDA-MB-231 and HeLa cells (Fig. S12). The endogenous expression level of MRs in the two cell lines was then determined by immunofluorescence staining (Fig. S13a and b) and real-time fluorescence quantitative PCR (RT qPCR) (Fig. S13c); the results indicated a significantly higher MR expression level in MDA-MB-231 than HeLa cells. Firstly, the cell uptake of MOF materials was evaluated using inductively coupled plasma mass spectrometry (ICP-MS). As shown in Fig. S14, the intracellular Fe levels were significantly higher in the **AMN/MIL-101-Man2** and **AMN/MIL-101-Man1**-treated cellular groups compared to that in the control group. Specifically, cells treated with **AMN/MIL-101**, **AMN/MIL-101-Man1** and **AMN/MIL-101-Man2** exhibited 3.8-fold, 9.4-fold and 10.5-fold increased Fe levels with respect to the control group, respectively. This demonstrates that the mannosyl MOFs can effectively target cells that overly express MR.

Subsequently, confocal laser-scanning microscopy was used for cell imaging (Fig. 3). The cells were first treated with free **AMN** or a MOF material (**AMN/MIL-101**, **AMN/MIL-101-Man1** and **AMN/MIL-101-Man2**) for 24 h to enable sufficient time for metabolic glycoengineering to occur, and then with **DBCO-FITC** (dibenzocyclooctyne-fluorescein isothiocyanate), a bioorthogonal fluorescent tag commonly used for labelling cell glycans.[31,32] We observed an evidently brighter fluorescence on the membrane of MDA-MB-231 cells after treatment with **AMN/MIL-101-Man1** and **AMN/MIL-101-Man2** than those treated with free **AMN** and **AMN/MIL-101** (Fig. 3a); fluorescence quantification of the images (Fig. 3b) confirmed that the fluorescence intensities quantified in the **AMN/ML1-101-Man1** and **AMN/MIL-101-Man2** groups are higher than those in the **AMN** and **AMN/MIL-101** groups. While **MIL-101-Man2** was used as a control to preclude false-positive labelling signals originating from empty MOFs, we found that the empty MOF did not enhance the fluorescence of **DBCO-FITC** labelling. In HeLa cells, no such fluorescence difference was observed among the four groups (**AMN**, **AMN/MIL-101**, **AMN/MIL-101-Man1**, and **AMN/MIL-101-Man2**) (Fig. 3c and d). These imaging results are in agreement with the endogenous MR expression levels of the two cell lines, suggesting the effectiveness of the mannosyl MOFs for MR-targeted delivery of **AMN** for glycoengineering.

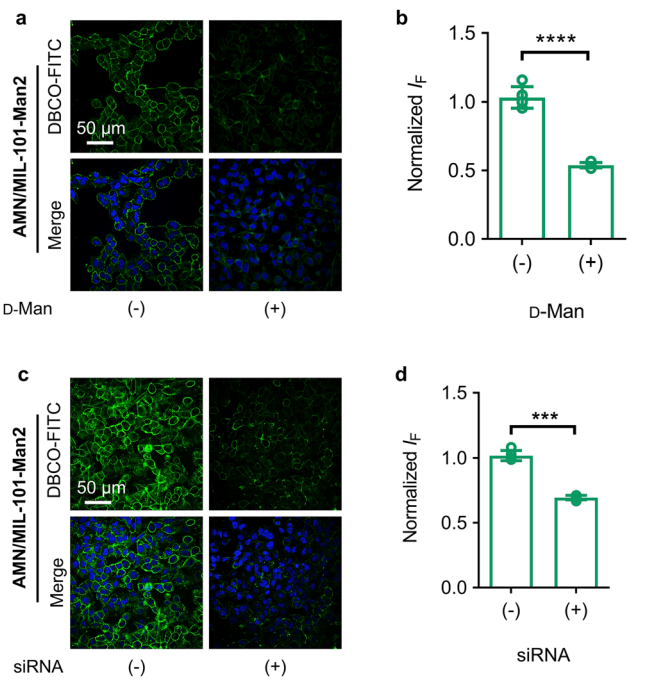

Fig. 4 Examining the MR-dependent metabolic glycoengineering of mannosyl MOFs. (a) Fluorescence imaging and (b) quantification of MDA-MB-231 cells treated with **AMN/MIL-101-Man2** in the absence (–) and presence (+) of 1 mM D-mannose (D-Man). (c) Fluorescence imaging and (d) quantification of MDA-MB-231 cells without and with pretreatment by an siRNA for interfering with the expression of endogenous CD206 (mannose receptor), followed by treatment with **AMN/MIL-101-Man2**. After treatment with the MOF for 24 h, cells were then treated with **DBCO-FITC** for 30 min for fluorescence labeling. Cell nuclei were stained with Hoechst 33342 (blue signal). Asterisks indicate significant differences (*$P < 0.05$, **$P < 0.01$, ***$P < 0.001$).

The **AMN/MIL-101-Man2** platform with enhanced targeting as evidenced by the confocal imaging was used for subsequent analyses. We treated MDA-MB-231 cells with different concentrations (5–40 μM, calculated using the **AMN** concentration) of **AMN/MIL-101-Man2** at 37 °C for 24 h (Fig. S15a and b). We observed that the fluorescence intensity became saturated at a concentration of 20 μM. By treating cells with the MOF material and monitoring over time (the cell culture medium was changed at each measurement point to remove excessive **AMN/MIL-101-Man2**), we observed a gradually enhancement of fluorescence on the cell membrane (Fig. S15c and d). These results indicated that the targeted glycoengineering is both concentration- and time-dependent.

To corroborate the MR targeting, a series of control experiments were conducted. MDA-MB-231 cells were treated with an excess of free D-mannose (D-Man) (1 mM) to adequately block the MRs on the cell surface. This was followed by incubation with **AMN/MIL-101-Man2**, and the results indicated a significantly decreased fluorescence intensity (Fig. 4a and b). Then, the cells were treated with an siRNA that causes degradation of endogenous mRNA of the MRs. RT qPCR showed a knockdown efficiency of 76% in MDA-MB-231 cells after RNA interference (Fig. S16). Subsequent imaging indicated that the labelling efficiency of the **AMN/MIL-101-Man2** delivery system decreased significantly in cells treated with the siRNA with respect to the raw cells (Fig. 4c and d). These experiments confirm the MR-dependent internalization of the mannosyl MOFs by MDA-MB-231 cells.

Finally, **AMN/MIL-101-Man2** was used for targeted glycoengineering in a co-cultured system as a proof-of-concept to demonstrate the applicability of the system for use in complex biological environments. The co-cultured system contains two transfected cell lines – MDA-MB-231 stably expressing mCherry fluorescent protein (referred to as mCherry-MDA-MB-231) and HeLa stably expressing TagBFP fluorescent protein (referred to as TagBFP-HeLa) (Fig. 5a). The cell lines were generated through lentivirus infection followed by puromycin selection (Fig. S17). Dual-channel fluorescence imaging indicated that the fluorescence of the two cell lines did not interfere with each other when co-cultured in one cellular medium (Fig. S17). We then incubated the cells with **AMN/MIL-101-Man2** or **AMN/MIL-101**, and then with **DBCO-FITC**, for triple-channel fluorescence imaging. Interestingly, we observed an intense fluorescence assigned to the **DBCO-FITC** label on the surface of mCherry-MDA-MB-231 cells but not in the adjacent TagBFP-HeLa cells (Fig. 5b). The fluorescence of FITC attached to the cell membrane of mCherry-MDA-MB-231 overlaps well with that of the intrinsic mCherry fluorescence (see the linear intensity quantification of cells). However, FITC fluorescence was hardly detected in TagBFP-HeLa cells. In addition, incubation of the cells with **AMN/MIL-101** resulted in minimal FITC fluorescence labelling being observed for either modified cell

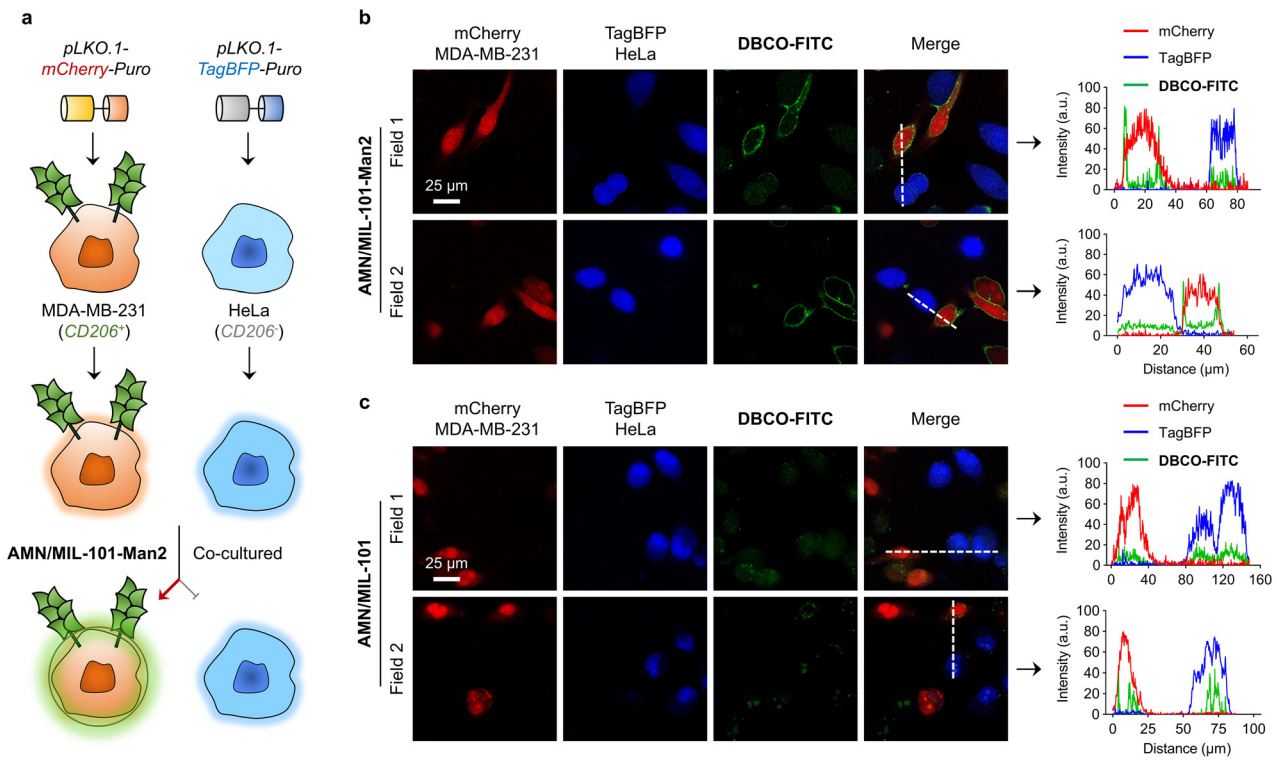

Fig. 5 **AMN/MIL-101-Man2** achieves targeted glycoengineering in a co-cultured system. (a) Schematic of targeted glycoengineering of **AMN/MIL-101-Man2** in a co-culture system. Fluorescence imaging and linear intensity quantification of co-cultured mCherry-MDA-MB-231 cells and TagBFP-HeLa cells treated with (b) **AMN/MIL-101-Man2** (20 μM/36 μg mL^{-1}) and (c) **AMN/MIL-101** (20 μM/35 μg mL^{-1}) for 24 h incubation, and then with **DBCO-FITC** (10 μM) for 30 min fluorescence labelling. The excitation/emission channel used for mCherry, TagBFP and **DBCO-FITC** is 561/580–620nm, 405/435–480 nm and 488/500–550 nm, respectively.

line (Fig. 5c). These results highlight the potential of the mannosyl MOFs for receptor-targeted delivery of **AMN** even in a co-cultured system.

Conclusions

In this study, we developed a cell-type selective metabolic glycan labeling tool based on mannosyl MOFs. The MOFs were readily prepared using a one pot method with mannose-functionalized ligands used for the coordination-driven self-assembly of MOFs. The as-constructed MOFs were demonstrated to be capable of effectively loading **AMN**, a non-natural sugar that could be metabolically incorporated into cellular glycans, and a series of fluorescence imaging assays confirmed the capacity of the mannosyl MOFs for the MR-targeted delivery of **AMN** to MDA-MB-231 cells that endogenously express a high level of MRs. Significantly, the ability of the material to achieve glycoengineering of a target cell in a bicellular system highlights its potential for glycobiological studies in complex biological samples. The targeting agent can also be flexibly replaced with other sugars for targeting a diverse range of sugar-binding proteins expressed on the surface of mammalian cells.[33,34]

Author contributions

P.-H. T. conceived the research. X.-P. H. and P.-H. T. designed the experiments. P.-H. T. performed most of the synthetic experiments. C. G. performed biological evaluation experiments. P.-H. T., C. G., X.-L. H., and X.-P. H. analyzed the data. P.-H. T., C. G., and X.-P. H. wrote the manuscript. X.-P. H., J. L., and T. D. J. discussed the data and revised the manuscript.

Conflicts of interest

There are no conflicts to declare.

Data availability

All data supporting the results of this study are available in the article or the supplementary information (SI) files. Supplementary information: Fig. S1–S17, Tables S1 and S2, NMR spectra, HRMS spectra, and further experimental details. See DOI: https://doi.org/10.1039/d5mh01986a.

Acknowledgements

The authors are thankful to the Natural National Science Foundation of China (NSFC) (No. 92253306, 82130099 and 22477030), the Science and Technology Commission of Shanghai Municipality (grant No. 24DX1400200), the International Cooperation Program of Shanghai Science and Technology (No. 23490711600), the Fundamental Research Funds for the Central Universities (222201717003), the Programme of Introducing Talents of Discipline to Universities (B16017), the National Natural Science Foundation of Shanghai Science and Technology (No. 24ZR1415400), the Shanghai Oriental Talents Youth Program (No. QNKJ2024010), the Shanghai Xuhui District Hospital Local Cooperation Project (23XHYD-20), the Open Funding Project of the State Key Laboratory of Fine Chemicals, Dalian University of Technology (KF 2402), State Key Laboratory of Chemo/Biosensing and Chemometrics, Hunan University, Changsha 410082, P. R. China, Ministry of Education Key Laboratory on signaling Regulation and Targeting Therapy of Liver Cancer (Naval Medical University) (grant 2023-MEKLLC-MS/ZD-00*) and the Shandong Laboratory Program (SYS202205) for financial support. T. D. J. wishes to thank the University of Bath and the Open Research Fund of the School of Chemistry and Chemical Engineering, Henan Normal University (2020ZD01), for support. The Research Center of Analysis and Test of East China University of Science and Technology is gratefully acknowledged for assistance in analytical experiments. We thank the staff members of the Integrated Laser Microscopy System at the National Facility for Protein Science in Shanghai for providing technical support and assistance in data collection and analysis.

References

1 M. Kufleitner, L. M. Haiber and V. Wittmann, *Chem. Soc. Rev.*, 2023, **52**, 510–535.
2 W. Huang and S. T. Laughlin, *Cell Chem. Biol.*, 2024, **31**, 409–427.
3 S. L. Scinto, D. A. Bilodeau, R. Hincapie, W. Lee, S. S. Nguyen, M. Xu, C. W. Am Ende, M. Finn, K. Lang and Q. Lin, *Nat. Rev. Method.*, 2021, **1**, 30.
4 B. Cheng, Q. Tang, C. Zhang and X. Chen, *Annu. Rev. Anal. Chem.*, 2021, **14**, 363–387.
5 W. Li, J. Guo, E. C. Hobson, X. Xue, Q. Li, J. Fu, C. X. Deng and Z. Guo, *Angew. Chem., Int. Ed.*, 2024, **63**, e202401921.
6 H. Wang, R. Wang, K. Cai, H. He, Y. Liu, J. Yen, Z. Wang, M. Xu, Y. Sun, X. Zhou, Q. Yin, L. Tang, I. T. Dobrucki, L. W. Dobrucki, E. J. Chaney, S. A. Boppart, T. M. Fan, S. Lezmi, X. Chen, L. Yin and J. Cheng, *Nat. Chem. Biol.*, 2017, **13**, 415–424.
7 H. Wang and D. J. Mooney, *Nat. Chem.*, 2020, **12**, 1102–1114.
8 R. Freitas, A. Peixoto, E. Ferreira, A. Miranda, L. L. Santos and J. A. Ferreira, *Biotechnol. Adv.*, 2023, **65**, 108144.
9 G. Xu, M. Wong, Q. Li, D. Park, Z. Cheng and C. B. Lebrilla, *Chem. Sci.*, 2019, **10**, 6992–7002.
10 A. Cioce, B. Calle, T. Rizou, S. C. Lowery, V. L. Bridgeman, K. E. Mahoney, A. Marchesi, G. Bineva-Todd, H. Flynn and Z. Li, *Nat. Commun.*, 2022, **13**, 6237.
11 W. Yi, P. Xiao, X. Liu, Z. Zhao, X. Sun, J. Wang, L. Zhou, G. Wang, H. Cao and D. Wang, *Signal Transduction Targeted Ther.*, 2022, **7**, 386.
12 R. Xie, S. Hong, L. Feng, J. Rong and X. Chen, *J. Am. Chem. Soc.*, 2012, **134**, 9914–9917.
13 R. Xie, L. Dong, Y. Du, Y. Zhu, R. Hua, C. Zhang and X. Chen, *Proc. Natl. Acad. Sci. U. S. A.*, 2016, **113**, 5173–5178.

14 Z. Liu, F. Wang, X. Liu, Y. Sang, L. Zhang, J. Ren and X. Qu, *Proc. Natl. Acad. Sci. U. S. A.*, 2021, **118**, e2022769118.
15 J. Yang, K. Yang, S. Du, W. Luo, C. Wang, H. Liu, K. Liu, Z. Zhang, Y. Gao, X. Han and Y. Song, *Angew. Chem., Int. Ed.*, 2023, **62**, e202306863.
16 P. Horcajada, T. Chalati, C. Serre, B. Gillet, C. Sebrie, T. Baati, J. F. Eubank, D. Heurtaux, P. Clayette and C. Kreuz, *Nat. Mater.*, 2010, **9**, 172–178.
17 P.-H. Tong, J.-J. Wang, X.-L. Hu, T. D. James and X.-P. He, *Chem. Sci.*, 2023, **14**, 7762–7769.
18 P.-H. Tong, J.-J. Yang, Y.-F. Zhou, Y.-F. Tang, M.-T. Tang, Y. Zang, Y.-F. Pan, L.-W. Dong, Y.-X. Tan and K. T. Nam, *Coord. Chem. Rev.*, 2025, **526**, 216381.
19 X. Chen, S. M. Argandona, F. Melle, N. Rampal and D. Fairen-Jimenez, *Chem*, 2024, **10**, 504–543.
20 Y. Wang, R. L. Foulkes, N. Panagiotou, P. Markopoulou, A. B. Popov, A. Eskandari, L. Fruk and R. S. Forgan, *J. Colloid Interface Sci.*, 2025, **681**, 416–424.
21 R. E. Giménez, E. Piccinini, O. Azzaroni and M. Rafti, *ACS Omega*, 2019, **4**, 842–848.
22 H. Zhang, Y. Shang, Y.-H. Li, S.-K. Sun and X.-B. Yin, *ACS Appl. Mater. Interfaces*, 2018, **11**, 1886–1895.
23 P.-H. Tong, L. Zhu, Y. Zang, J. Li, X.-P. He and T. D. James, *Chem. Commun.*, 2021, **57**, 12098–12110.
24 J. Hu, W. Wu, Y. Qin, C. Liu, P. Wei, J. Hu, P. H. Seeberger and J. Yin, *Adv. Funct. Mater.*, 2020, **30**, 1910084.
25 L. Wei, X. Xu, K. Xi, L. Zhang, X. Cheng, Y. Lan, S. Jiang, Y. Lei, J. Yin and H. Wu, *J. Alloys Compd.*, 2023, **968**, 172063.
26 L. Feng, K.-Y. Wang, G. S. Day, M. R. Ryder and H.-C. Zhou, *Chem. Rev.*, 2020, **120**, 13087–13133.
27 F. Leng, S. Sun, Y. Jing, F. Wang, Q. Wei, X. Wang and X. Zhu, *Bulg. Chem. Commun.*, 2016, **48**, 109–113.
28 X. Xia, D.-e Sun, Q. Tang, X. Liu, X. Fan, Y. Wan, S. Cui, X. Zhang, Q. Liu and Y. Jiang, *J. Am. Chem. Soc.*, 2024, **146**, 22008–22016.
29 L. Feng, S. Hong, J. Rong, Q. You, P. Dai, R. Huang, Y. Tan, W. Hong, C. Xie and J. Zhao, *J. Am. Chem. Soc.*, 2013, **135**, 9244–9247.
30 X. Niu, H. Yang, J. Guo, L. Yao, Y. Wang, W. Yu, Z. Liu and H. Chen, *Adv. Healthcare Mater.*, 2024, **13**, 2400970.
31 B. Hou, J. Ye, L. Huang, W. Cheng, F. Chen, H. Zhou, J. Pan, J. Gao, Y. Lai and Y. Zhao, *Sci. Adv.*, 2024, **10**, eadq3940.
32 R. Bhatta, J. Han, J. Zhou, H. Li and H. Wang, *J. Controlled Release*, 2022, **347**, 164–174.
33 X.-P. He and H. Tian, *Chem*, 2018, **4**, 246–268.
34 X.-P. He, *Chem. Soc. Rev.*, 2026, **55**, 605–618.

